ADVANCED THERAPEUTICS
www.advtherap.com

Transferrin-Coated Nanodiamond–Drug Conjugates for Milliwatt Photothermal Applications

*Sean Harvey, Marco Raabe, Anna Ermakova, Yingke Wu, Todd Zapata, Chaojian Chen, Hao Lu, Fedor Jelezko, David Y. W. Ng, and Tanja Weil**

Fluorescent nanodiamonds (fNDs) are unique carbon-based nanomaterials due to their outstanding optical and magnetic properties. However, realization of the full potential of fNDs is often limited by their processability because fNDs aggregate strongly in both organic and aqueous solutions. Therefore, robust and potentially universal coating strategies are urgently needed to address these limitations. Derived from mussel foot proteins, the polymerization of L-3,4-dihydroxyphenylalanine (L-DOPA) provides important surface functional groups including amines, carboxylic acid, alcohols, and conjugated Michael acceptors. Herein, L-DOPA is polymerized on fNDs with a high control over the shell thickness. Photoluminescence and optically detected magnetic resonance studies reveal that the unique photophysical properties of fNDs are preserved after thin poly(L-DOPA) film coating. Subsequently, conjugation of transferrin, a heme protein that provides efficient receptor-specific cellular transport, improves the colloidal stability and cellular uptake of the poly(L-DOPA)-coated fNDs. The loading of FDA-approved indocyanine green as a photothermal agent yields an integrated biohybrid material exhibiting an amplified photothermal effect in cells at very low energy intake (≈90 mW cm^{-2}).

1. Introduction

Among carbon-based materials, fluorescent nanodiamonds (fNDs) are unique as they do not only possess excellent photoluminescence properties, but they are also very precise local sensors of magnetic and electric fields, temperature, or mechanical forces.[1,2] These characteristics are predominantly derived from the defect centers in nanodiamonds (NDs) where impurity atoms such as nitrogen,[3] silicon,[4,5] and germanium[6] are localized alongside lattice vacancies. Consequently, the type of such crystallographic defects defines its unique optical spectrum as well as spin properties. Hence, the optical behavior of fNDs is independent of its size, in contrast to other classes of nanoemitters such as quantum/carbon dots and gold nanoparticles.[7] The best studied color center is the nitrogen-vacancy (NV) center.[2,3,8–11] The remarkable properties of this atom-like defect in the diamond lattice allow application for high-resolution magnetic (bio)sensing,[12] energy transfer,[13] bioimaging,[12] and even quantum computing technologies.[14] Due to this, in the present work, nanodiamonds with NV centers were selected as base material for designing a potent theranostic system.

In order to achieve these aims, the processability of NDs is a recurring challenge. The colloidal stability of NDs in solution, both organic and aqueous, is extremely poor and is further aggravated with the reduction in the size of the diamond particle.[9,15] Hence, the capability to chemically introduce novel functions tends to be severely hampered by the aggregation of the NDs. To alleviate this primary issue, nanodiamond coating technologies have been developed using adsorption mechanisms deriving from weak attractive forces (electrostatic, van der Waals, hydrogen bonding) and/or strong covalent interactions.[8,16,17] However, these coating technologies have persistent difficulties due to batch to batch production variability impacting the surface composition of NDs. In addition, it is crucial to understand that the coating material has to fulfill many important criteria, including 1) chemical multifunctionality, 2) reproducibility of the coating strategy on NDs from different sources and sizes, 3) colloidal stability of the fND conjugate in biological media and inside cells, and 4) minimally affecting the photoluminescence and magnetic sensing capabilities.

S. Harvey, M. Raabe, Dr. A. Ermakova, Y. Wu, Dr. T. Zapata, C. Chen, Dr. H. Lu, Dr. D. Y. W. Ng, Prof. T. Weil
Max Planck Institute for Polymer Research
Ackermannweg 10, 55128 Mainz, Germany
E-mail: weil@mpip-mainz.mpg.de
S. Harvey, M. Raabe, C. Chen, Prof. T. Weil
Institute of Inorganic Chemistry I
Ulm University
Albert-Einstein-Allee 11 89081 Ulm, Germany
Prof. F. Jelezko
Institute for Quantum Optics
Ulm University
Albert-Einstein-Allee 11 89081 Ulm, Germany
The ORCID identification number(s) for the author(s) of this article can be found under https://doi.org/10.1002/adtp.201900067

DOI: 10.1002/adtp.201900067

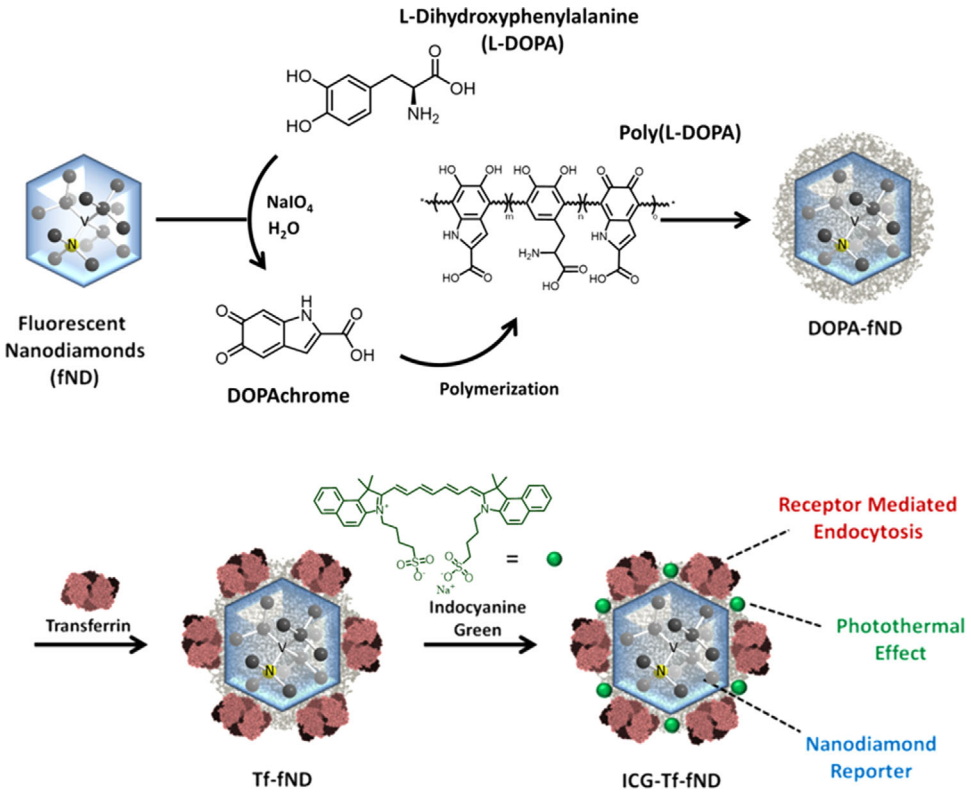

Figure 1. Schematic illustration of fND nanosystem preparation.

While it is synthetically challenging for a coating methodology that performs consistently well regardless of surface properties, nature has aptly demonstrated otherwise. Derived from mussel foot proteins, the polymerization of catechol pendant groups is the key for the attachment of mussel bivalves onto virtually any surface. Messersmith et al. first showed that polymers of catecholamines, in particular dopamine, can replicate the adhesiveness of the mussel foot.[18] The significance of polydopamine was quickly realized resting on its capability to adapt to various surface functions. This behavior was also observed for other catecholamines, such as L-3,4-dihydroxyphenylalanine (L-DOPA)[19–22] and norepinephrine.[23–25] Chemically, polycatecholamine films possess important functional groups including amines, alcohols, and conjugated Michael acceptors leading to a massive variety of post-functionalized surfaces.[18,26,27] In this context, polydopamine has been demonstrated recently as a proof of concept to functionalize NDs.[28,29] Polydopamine–ND systems represent an attractive platform. However, post-functionalization with, for example, polyethylene glycol has been crucial due to the high adhesiveness of polydopamine that potentially contributes to the aggregation of the coated nanodiamonds, especially under physiological buffer conditions.[30] In comparison, L-DOPA contains an additional carboxylic group giving poly(L-DOPA) coatings a higher hydrophilicity compared to polydopamine.[18,19]

Herein, we show that poly(L-DOPA) does not only act as a polar and versatile bridging entity to conjugate multiple functional entities onto fNDs but also enhances its photothermal capability to develop a complex fND therapeutic platform (**Figure 1**). Furthermore, we establish the strategy of polymerization of L-DOPA on fNDs from different sources (FND Biotech, Microdiamant) by monitoring the kinetics of polymerization, the control over thickness and colloidal stability under physiological conditions. The effect of the poly(L-DOPA) coating on the photoluminescence and optically detected magnetic resonance were studied, and these unique photophysical properties were preserved for fNDs with thin surface coating. Subsequently, the coated fNDs were further decorated by transferrin, a heme cell membrane protein involved in receptor-specific cellular uptake that stabilizes the biohybrid in cellular media and the FDA-approved indocyanine green (ICG) as a photothermal agent. By localizing a high concentration of ICG in cellular vesicle nanoenvironments, we envision that the integrated material will provide high photothermal toxicity even at very low energy intake.

2. Results and Discussion

2.1. Preparation and Characterization of L-DOPA-Coated Nanodiamonds

Nanodiamonds with 35 nm average diameter were purchased from FND Biotech (Taiwan) and used without further surface treatment. Sodium periodate initiated polymerization of dopamine, and L-DOPA in pure MilliQ water was used to avoid buffer salts, which are known to destabilize colloidal NDs.[15] In addition, this method provides faster deposition times than polymerization in alkaline buffers[31–33] further reducing ND aggregation. In contrast to the well-established dopamine surface

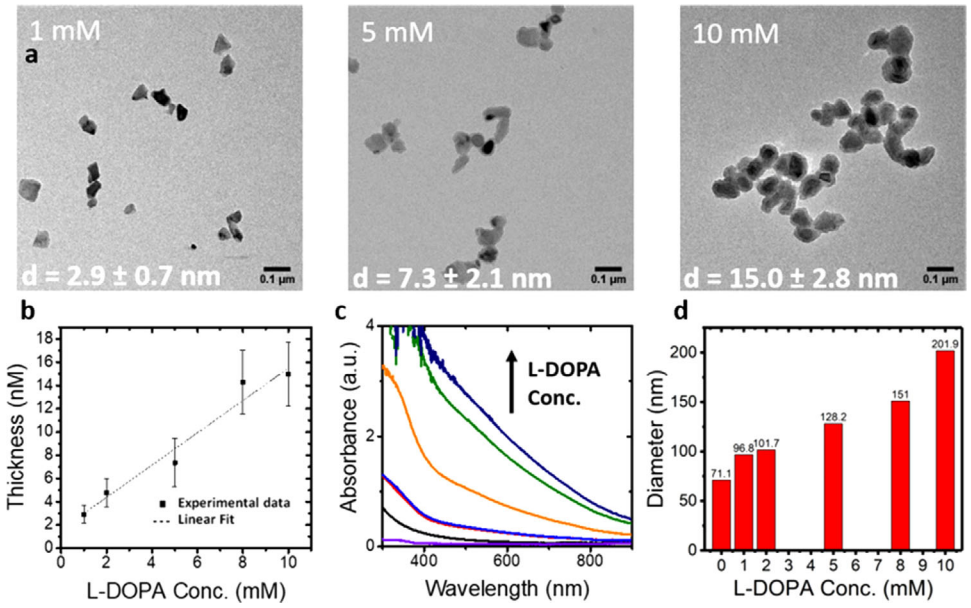

Figure 2. a) Transmission electron microscope images of DOPA-fND prepared with different concentrations of L-DOPA. Data presented as mean ± SEM, $n = 44$. b) Poly(L-DOPA) shell thickness increases linearly with L-DOPA concentration ($n = 44$). c) UV–vis absorption spectra of aqueous solutions of DOPA-fND (100 µg mL^{-1}) showing broadband absorbance into the NIR. d) Dynamic light scattering data. Hydrodynamic diameter of DOPA-fND increases with increasing L-DOPA concentrations.

polymerization, L-DOPA provides an additional carboxylic group and poly(L-DOPA) coatings exhibit higher hydrophilicity than polydopamine.[20,21] We anticipate that poly(L-DOPA) would show a greater potential in enhancing the aqueous stability of fNDs. In our experimental setup, 100 µg fNDs were dispersed in MilliQ water under sonication. To this solution was added a volume of freshly prepared L-DOPA or dopamine (2.5 mg mL^{-1}) solution in MilliQ to bring the final catecholamine concentration to 1–10 mM. This mixture was heated to 55 °C and sonicated for 5 min to ensure thorough mixing. Finally, an appropriate volume of freshly prepared sodium periodate solution (10.84 mg mL^{-1}) was added to give 0.5 molar equivalents (sodium periodate to catecholamine) and bring the final volume to 1 mL. The solution was sonicated for further 5 min at 55 °C. The reaction was continued on a shaker at 500 rpm for additional 15 min. The coated fNDs were purified by five centrifugation and washing cycles through an ultrafiltration tube (100 kDa). UV–vis spectroscopy showed that unreacted monomer and excess oxidation products were removed after three cycles (Figure S1e, Supporting Information). While fNDs coated in the L-DOPA were colloidally stable, fNDs coated with polydopamine exhibited a high degree of aggregation, lower polymerization efficiency, and poorer aqueous stability (Figures S1 and S12, Supporting Information). The applicability of the L-DOPA coating methodology was evaluated under transmission electron microscopy with three different batches and two different sources of fNDs (FND Biotech, Microdiamant) yielding the DOPA-fNDs (**Figure 2**a and Figure S2, Supporting Information). The poly(L-DOPA) coating can be clearly seen on each fND, which are well dispersed across the TEM grid with small aggregates attributed to drying effects (Figure 2a,b and Figure S2, Supporting Information). The poly(L-DOPA) coating was further confirmed by dynamic light scattering (DLS; Figure S12, Supporting Information), X-ray photoelectron spectroscopy (XPS), and Raman and Fourier transform Infrared (FT-IR) spectroscopies demonstrating a positive outlook toward its applicability across different ND sources (Figure 2d and Figures S3–S5, Supporting Information). In addition, the polymerization method allows controlling the thickness of poly(L-DOPA) by simply varying the concentration of the monomer. Between 1–10 mM of L-DOPA, the thickness varies linearly from 3–15 nm, suggesting that the synthesis is robust and predictable. The aforementioned thicknesses were simultaneously characterized by the absorbance of poly(L-DOPA), DLS, and TEM (Figure 2). DOPA$_{15nm}$-fND with 15 nm shell thickness was obtained using 10 mM L-DOPA, and XPS was used to elucidate molecular information and ascertain the bonds formed during polymerization. Against pure fND, L-DOPA, and poly(L-DOPA) as controls, the characteristic signals from the C—N—C, C═N—C bonds clearly demonstrate the cyclization of L-DOPA as an intermediate into its polymeric form (Figure S3, Supporting Information). Moreover, the relative photoelectron count of the C–O, C═O, C—C$_{sp3}$, and C—C$_{sp2}$ signals indicate contributions from both the fND surface as well as from poly(L-DOPA). As the polymerization of L-DOPA proceeds via a radical mechanism,[26,34] it is essential to characterize the influence of the coating toward the magnetic properties of the fND.

2.2. Physical Properties of L-DOPA Coated Nanodiamonds

In this respect, the effect of poly(L-DOPA) with two different thicknesses (3 and 15 nm) to the NV's properties in fNDs was investigated. Spectra measurements were performed on a custom-built confocal microscope with the excitation laser light at 515 and 532 nm. The spectra of coated fNDs reveal that the poly(L-DOPA) layer adds a unique background signal (**Figure 3**a). The

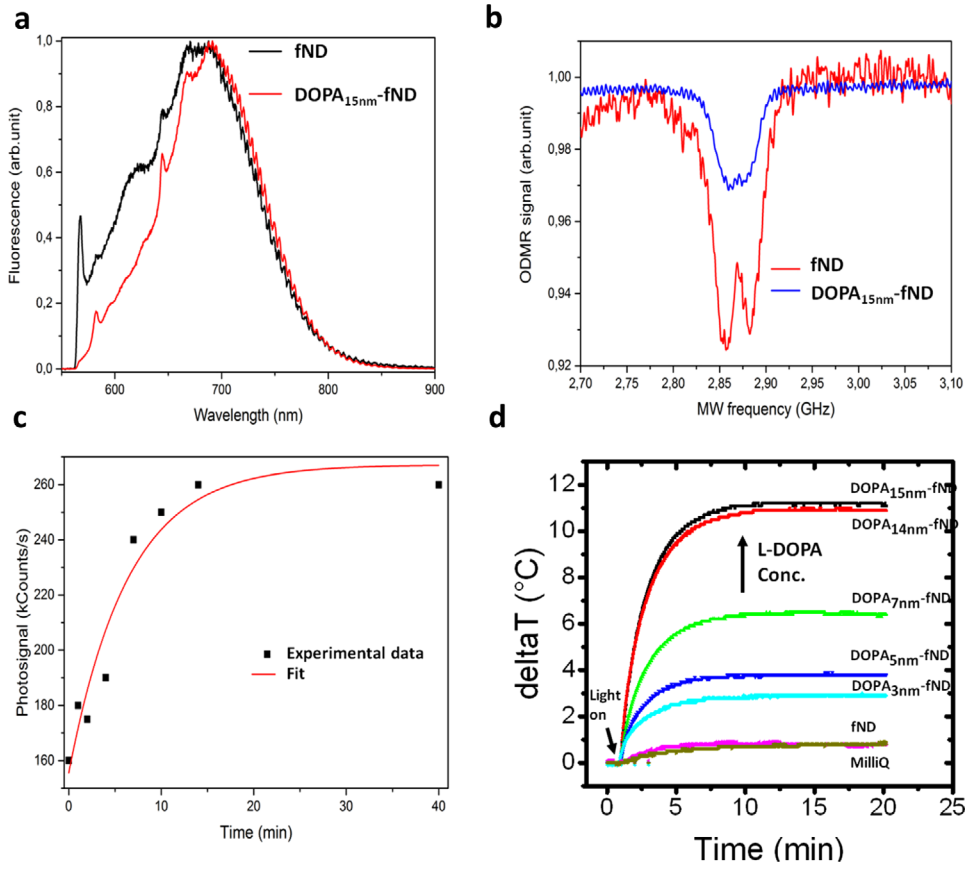

Figure 3. a) Normalized emission spectra (ex. 532 nm) for fND and $DOPA_{15nm}$-fND. NV^0 and NV^- zero phonon lines are visible in both spectra. Fluorescence of poly(L-DOPA) coating evident between 570 and 700 nm. b) Nanodiamonds with PDA layer (15 nm) demonstrate stable ODMR lines; however, the presence of PDA layer decrease the contrast of ODMR. It can be related to background fluorescence from PDA. c) The fluorescence of DOPA-fND increases with time of laser illumination. Fluorescence increase is stable in time. d) Temperature increase of aqueous solutions of various concentrations of DOPA-fND (100 μg mL^{-1} fND) after near-infrared (NIR) irradiation (810 nm lamp; 1 W cm^{-2}).

intensity of the background signal depends on the thickness of the layer but the zero phonon lines of NV^- and NV^0 centers are well visible in each sample. A decrease in the initial fluorescence intensity proportional to the coating thickness was observed for DOPA-fND (Figure S6, Supporting Information) attributed to the broadband absorbance of polycatecholamines. Unexpectedly, independent of the wavelength of the laser light, the detected fluorescence increased over 60% from the initial excitation and reached saturation level within a few minutes (Figure 3c) as measured for 20 $DOPA_{15nm}$-fND. The high level of fluorescence is stable in time after cessation of laser excitation and remains so even after 4 h in darkness (Figures S7 and S8, Supporting Information), which enables more advanced imaging with tracking of nanodiamonds without double counting of the same particle.

To study the charge properties of NV centers in fNDs, optically detected magnetic resonance (ODMR) was observed. Resolved ODMR lines (Figure 3b) prove the presence of NV^- centers in NDs after poly(L-DOPA) coating, indicating its suitability for sensing applications. The decrease of ODMR contrast is attributed to background light from the poly(L-DOPA) layer. However, deeper investigations of the spin properties of NV center in poly(L-DOPA)-coated NDs are currently ongoing.

Due to the presence of oligomeric and polymeric components of various order within the structure, polycatecholamines are good energy absorbers from UV to NIR.[26,35–37] Furthermore, absorbed light is converted to heat with high efficiency allowing their application as photothermal agents.[38] Photothermal agents that are active in the NIR range are of greater interest due to the reduced absorbance by the body in this region.[39,40] We demonstrated that all poly(L-DOPA)-coated fNDs exhibited an enhanced photothermal effect over pure fNDs when irradiated at 810 nm, and achieving greater than 10-fold increase (ΔT = 11.1 °C vs 0.8 °C) in temperature change for $DOPA_{15nm}$-fND (Figure 3d). Although, a higher photothermal effect was observed for $DOPA_{15nm}$-fND, we chose to continue our experiments with $DOPA_{7nm}$-fND (ΔT = 6.4 °C) providing an appropriate balance between fluorescence intensity and photothermal effects.

2.3. Post-Modification of DOPA-fND for Uptake Studies In Vitro

To investigate the poly(L-DOPA) coating as a homogenized platform for the post-functionalization of fNDs, we examined the conjugation of proteins as stabilizing and biologically active functional entities.[41–43] As a conserved 3D structure of the adsorbed

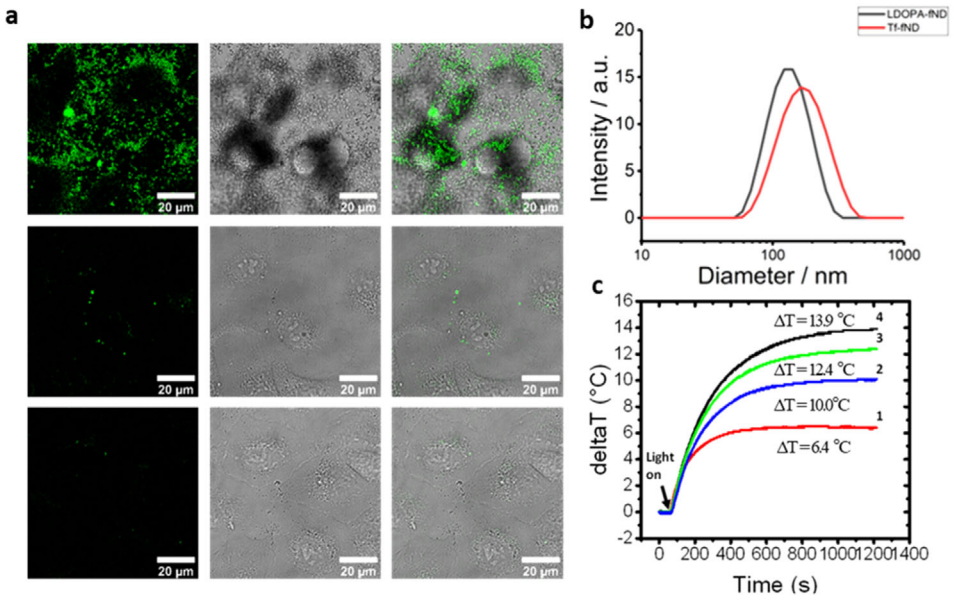

Figure 4. a) Confocal microscopy images of uptake of $DOPA_{7nm}$-fND (top row) and Tf-fND (middle) in A549 cells (250 μg mL^{-1}). Significant aggregation and sedimentation of $DOPA_{7nm}$-fND visible. Tf-fND uptaken without sedimentation. Bottom row is blank sample. b) Dynamic light scattering data for $DOPA_{7nm}$-fND and Tf-fND. c) Temperature increase of aqueous solutions of $DOPA_{7nm}$-fND (100 μg mL^{-1}) (1), free ICG (100 and 200 μg mL^{-1}) (2 and 3), and ICG-Tf-fND (100 μg mL^{-1}; 190 μg mL^{-1} ICG equiv) (4) after near-infrared (NIR) irradiation (810 nm lamp; 1 W cm^{-2}).

protein is essential for its activity, the impact of its conjugation onto the poly(L-DOPA) coating can be directly assessed in a biological assay system.

Human transferrin (Tf, 79.5 kDa), a heme-containing protein that binds and transports iron through transferrin receptors expressed at the membrane of many cells and has been used to enhance the uptake of nanoparticles,[44,45] was loaded directly onto DOPA-fND by mixing overnight in a mildly alkaline phosphate buffer. Adsorption of transferrin to the surface was likely accomplished through a combination of non-covalent interactions and covalent bonding via the amine-reactive Michael acceptors or carbonyls (Schiff base) of the quinone moieties formed during the polymerization of L-DOPA (Figure S13, Supporting Information), which has been also discussed before for L-DOPA polymers.[46] Unbound protein was removed from the reaction mixture by ultrafiltration (molecular weight cut off = 100 kDa) to afford Tf-fND. Upon loading, the hydrodynamic radius increased from 63 nm for DOPA-fND, to ≈78 nm for Tf-fND, indicating the successful formation of a protein corona around the fND (**Figure 4**b). Successful loading was also confirmed by FT-IR (Figure S9, Supporting Information). The capability of transferrin to initiate receptor-mediated endocytosis of Tf-fND was evaluated using A549 lung adenocarcinoma cell line. In contrast to fND alone or the precursor DOPA-fND, efficient receptor-mediated uptake of Tf-fND was observed through confocal laser scanning microscopy (Figure 4a). Next, we adsorbed ICG, a small molecule dye with innate photothermal properties, onto Tf-fND. The loading of ICG onto Tf-fND was accomplished by overnight incubation of Tf-fND and ICG in the dark with subsequent removal of excess ICG through extensive ultrafiltration to afford ICG-Tf-fND. The amount of ICG loaded was determined through its characteristic absorbance at 400 nm and found to be >180% by mass compared to the fND (1.89 mg mg^{-1} fND). In this way, a high local concentration of ICG was obtained, which could enhance the photothermal effect of poly(L-DOPA)-coated fNDs. Subsequently, we quantify the photothermal effect of ICG-Tf-fND by observing the differential temperature increase in water upon irradiation at 810 nm. In comparison to $DOPA_{7nm}$-fND (ΔT = 6.4 °C) and ICG (ΔT = 12.4 °C), ICG-Tf-fND (ΔT = 13.9 °C) showed a 120% and 12% improvement, respectively, in terms of temperature increase attained after 20 min of irradiation (Figure 4c). Comparing absolute ICG concentrations, the magnitude difference in temperature profile produced by ICG-Tf-fND suggests that there is an enhancement for the loaded ICG over that of molecularly free ICG. This amplified photothermal effect by confinement was also characteristically observed in hollow inorganic nanoparticles and plasmonic nanoparticle clusters.[47,48] The strong interaction of ICG with Tf-fND was demonstrated by the negligible release of ICG (<5%) from ICG-Tf-fND when incubated in cell media for 24 h (Figure S10, Supporting Information).

2.4. Photothermal Applications In Vitro

We subsequently evaluated ICG-Tf-fND in HeLa and A549 cells. The internalization pathway of ICG-Tf-fND was elucidated by confocal microscopy. The fluorescence signal from ICG (ex. 561 nm, em. 750–800 nm) was imaged. It is interesting to note that the transport of ICG-Tf-fND is represented in a receptor-mediated manner by formation of endosomal vesicles where the fluorescence signals are highly localized (Figure S11, Supporting Information) and no freely diffusing ICG are obtained.

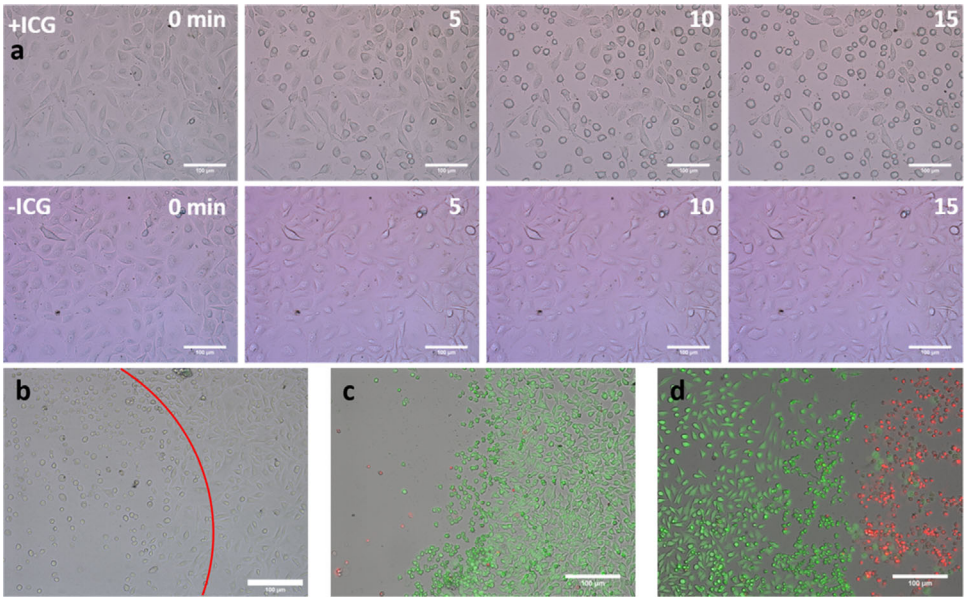

Figure 5. a) Optical images (20 ×) of HeLa cells incubated overnight with ICG-Tf-fND and Tf-fND at 0, 5, 10, and 15 min after irradiation with 810 nm lamp, 430 mW cm^{-2}. Cell rounding is evident within 5 min in ICG-Tf-fND sample. No morphological changes observed with Tf-fND after 15 min. Scale bar = 100 µm. b) Brightfield image (10 ×) of A549 cells incubated overnight with ICG-Tf-fND imaged 4 h after 15 min irradiation with 810 nm lamp, 90 mW cm^{-2}. Border (marked with red line) between irradiated area and non-irradiated area clearly visible. Scale bar = 100 µm. c) Live and dead staining (10 ×) of HeLa cells incubated overnight with ICG-Tf-fND imaged 4 h after 15 min irradiation with 810 nm lamp, 430 mW cm^{-2}. Dead cells were washed away during preparation leaving an empty region bordered by healthy cells. Scale bar = 100 µm. d) Live and dead staining (10 ×) of HeLa cells incubated overnight with ICG-Tf-fND imaged 4 h after 15 min irradiation with 810 nm lamp, 4 W cm^{-2}. Sharp border clearly observed between live (green) and dead (red) cells. Scale bar = 100 µm.

Molecularly, free ICG rampantly diffuses throughout the cell (Figure S11, Supporting Information), clearly different to ICG-Tf-fND, which also indicates the strong interaction between ICG and Tf-fND.

Upon internalization, the photothermal effect was initiated using an 810 nm lamp (200 mW) concentrated through the objective onto the sample area. Light densities were varied by the magnification of the objective (10 ×, 20 ×, 40 ×) and supplied current. Simultaneously, time-lapsed optical images were recorded in 20 s intervals to visualize the morphological changes due to the localized heating effect by ICG-Tf-fND. First, various light densities (0.09, 0.4, and 4.0 W cm^{-2}) for the irradiation process were conducted to identify the optimum power for photothermal-induced cytotoxicity within 15 min. Efficient and immediate cell rounding (under 5 min) was visually observed at light densities of 0.4 and 4.0 W cm^{-2} (**Figure 5**a and Movies S1 and S2, Supporting Information). Even very low light densities down to 0.09 W cm^{-2} induced cell rounding visually detected within 10 min with cell death thereafter (Figure 5b and Movie S3, Supporting Information), a remarkably low power density compared to the previously reported ICG–polydopamine–ND conjugate which required over an order of magnitude higher power (2 W cm^{-2}).[29] Live/dead staining of the cells using fluorescein diacetate/propidium iodide combination further demonstrates the characteristic spatial control of the light-induced cell death (Figure 5c,d). In comparison, no cell death and only minor morphological changes upon irradiation were observed for Tf-fND or fND + ICG mixture at any power density (Figure 5a and Movies S4 and S5, Supporting Information).

3. Conclusion

In summary, we have described a hierarchical construction of a nanodiamond-based theranostic system through a poly(L-DOPA) coating that serves as a sticky layer for chemical functionalization. By selecting the protein transferrin and the small molecule dye ICG as two biologically active molecular components, we demonstrate that the poly(L-DOPA) is an excellent avenue for post-modification with both small molecules and proteins. Notably, the poly(L-DOPA) coating stabilizes the optical properties of NV centers in the nanocrystals, and at the same time, it has no negative effects on the charge state of NV^- defects, which is crucial for future imaging and sensing applications.

Critical for effective dosing of deep-seated tumors due to the exponential attenuation of light, the activation threshold for the photothermal effect was at least ten times lower compared to other nanodiamond-based systems.[49–52] The endocytic transport behavior and the immediate cellular response toward localized heating, observed in confocal and time-lapsed microscopy, clearly demonstrate the efficiency of the system.

Compared to other fluorescent nanoparticles, fNDs have shown promise for in vitro and in vivo application due to their high photostability. Tracking of particles in real time over long periods can reveal information about biodistribution whereas the defect centers (e.g., NV^-, Si) enable sensing of temperature as a nanoscale thermometer to monitor photothermal effects in situ. To date, nanodiamonds have already been applied successfully in vivo for many animal models (mouse,[16] chicken embryo,[53] and miniature pig[54]).[55]

We envision that the combination of optical and magnetic detection and ultra-low power density required for phototoxicity could open new avenues to the noninvasive treatment of malignant tumors deep within the body, which could reach tissue in the brain, prostate, colorectal, and pancreas. Collectively, the presented methodology rapidly facilitates the general preparation of customized multifunctional fNDs, in which a broad selection of functional components such as proteins and drugs could be used in combination.

Supporting Information

Supporting Information is available from the Wiley Online Library or from the author.

Acknowledgements

S.H. and M.R. contributed equally to this work. This project was funded by the ERC Synergy grant 319130-BioQ, the European Union's Horizon 2020 project "Hyperdiamond" under the grant agreement No 667192, the Collaborative Research Center (CRC) Transregio 234 (project B4), and the Deutsche Forschungsgemeinschaft (DFG, German Research Foundation) under project number 316249678 (SFB 1279, project C1, C4). Y.W. thanks the China Scholarship Council (CSC) for funding and C.C. is grateful for a doctoral fellowship from Promotionskolleg Pharmaceutical Biotechnology of Ulm University funded by the state of Baden-Württemberg.

Conflict of Interest

The authors declare no conflict of interest.

Keywords

L-DOPA, mussel-inspired, nanodiamonds, photothermal therapy, theranostics, transferrin

Received: May 13, 2019
Revised: July 7, 2019
Published online: August 16, 2019

[1] V. N. Mochalin, O. Shenderova, D. Ho, Y. Gogotsi, *Nat. Nanotechnol.* **2012**, *7*, 11.
[2] Y. Wu, F. Jelezko, M. B. Plenio, T. Weil, *Angew. Chem., Int. Ed.* **2016**, *55*, 6586.
[3] R. Schirhagl, K. Chang, M. Loretz, C. L. Degen, *Annu. Rev. Phys. Chem.* **2014**, *65*, 83.
[4] R. L. Walsworth, H. Zhang, I. Aharonovich, J. W. Lichtman, D. R. Glenn, R. Schalek, E. L. Hu, A. P. Magyar, *Small* **2014**, *10*, 1908.
[5] S. Choi, V. Leong, V. A. Davydov, V. N. Agafonov, M. W. O. Cheong, D. A. Kalashnikov, L. A. Krivitsky, *Sci. Rep.* **2018**, *8*, 3792.
[6] T. Inubushi, N. Mizuochi, F. Ishibashi, M. Hatano, Y. Doi, Y. Miyamoto, L. J. Rogers, S. Kobayashi, S. Yamasaki, F. Jelezko, S. Nagamachi, B. Naydenov, K. Tahara, K. D. Jahnke, T. Iwasaki, T. Miyazaki, *Sci. Rep.* **2015**, *5*, 12882.
[7] M. H. Alkahtani, F. Alghannam, L. Jiang, A. Almethen, A. A. Rampersaud, R. Brick, C. L. Gomes, M. O. Scully, P. R. Hemmer, *Nanophotonics* **2018**, *7*, 1423.
[8] M. Chipaux, K. J. van der Laan, S. R. Hemelaar, M. Hasani, T. Zheng, R. Schirhagl, *Small* **2018**, *14*, 1704263.
[9] K. van der Laan, M. Hasani, T. Zheng, R. Schirhagl, *Small* **2018**, *14*, 1703838.
[10] S. Claveau, J. R. Bertrand, F. Treussart, *Micromachines* **2018**, *9*, 1.
[11] D. Ho, C.-H. K. Wang, E. K.-H. Chow, *Sci. Adv.* **2015**, *1*, e1500439.
[12] W. W. W. Hsiao, Y. Y. Hui, P. C. Tsai, H. C. Chang, *Acc. Chem. Res.* **2016**, *49*, 400.
[13] A. Nagl, S. R. Hemelaar, R. Schirhagl, *Anal. Bioanal. Chem.* **2015**, *407*, 7521.
[14] S. Mouradian, B. Lienhard, M. Walsh, H. Bakhru, B. J. Shields, T. Schröder, D. Englund, D. Kim, N. H. Wan, *Nano Lett.* **2018**, *18*, 2787.
[15] S. R. Hemelaar, A. Nagl, F. Bigot, M. M. Rodríguez-García, M. P. de Vries, M. Chipaux, R. Schirhagl, *Microchim. Acta* **2017**, *184*, 1001.
[16] M. D. Torelli, A. G. Rickard, M. V. Backer, D. S. Filonov, N. A. Nunn, A. V. Kinev, J. M. Backer, G. M. Palmer, O. A. Shenderova, *Bioconjugate Chem.* **2019**, *30*, 604.
[17] D. Wang, Y. Tong, Y. Li, Z. Tian, R. Cao, B. Yang, *Diamond Relat. Mater.* **2013**, *36*, 26.
[18] H. Lee, S. M. Dellatore, W. M. Miller, P. B. Messersmith, *Science* **2007**, *318*, 426.
[19] S. Azari, L. Zou, *J. Membr. Sci.* **2012**, *401–402*, 68.
[20] J. Kuang, J. L. Guo, P. B. Messersmith, *Adv. Mater. Interfaces* **2014**, *1*, 1400145.
[21] L. Yu, X. Liu, W. Yuan, L. J. Brown, D. Wang, *Langmuir* **2015**, *31*, 6351.
[22] H. Guo, Y. Sun, X. Niu, N. Wei, C. Pan, G. Wang, H. Zhang, H. Chen, T. Yi, X. Chen, *J. Chromatogr. A* **2018**, *1578*, 91.
[23] S. M. Kang, J. Rho, I. S. Choi, P. B. Messersmith, H. Lee, *J. Am. Chem. Soc.* **2009**, *131*, 13224.
[24] Y. Liu, G. Zhou, Z. Liu, M. Guo, X. Jiang, M. Berat Taskin, Z. Zhang, J. Liu, J. Tang, R. Bai, F. Besenbacher, M. Chen, C. Chen, *Sci. Rep.* **2017**, *7*, 8197.
[25] S. Hong, J. Kim, Y. Suk Na, J. Park, S. Kim, K. Singha, G.-I. Im, D.-K. Han, W. Jong Kim, H. Lee, *Angew. Chem., Int. Ed.* **2013**, *52*, 9187.
[26] J. Yang, M. A. Cohen Stuart, M. Kamperman, *Chem. Soc. Rev.* **2014**, *43*, 8271.
[27] J. H. Ryu, P. B. Messersmith, H. Lee, *ACS Appl. Mater. Interfaces* **2018**, *10*, 7523.
[28] Y. Zeng, W. Liu, Z. Wang, S. Singamaneni, R. Wang, *Langmuir* **2018**, *34*, 4036.
[29] D. Maziukiewicz, B. Grześkowiak, E. Coy, S. Jurga, R. Mrówczyński, *Biomimetics* **2019**, *4*, 3.
[30] H.-S. Jung, K.-J. Cho, Y. Seol, Y. Takagi, A. Dittmore, P. A. Roche, K. C. Neuman, *Adv. Funct. Mater.* **2018**, *28*, 1801252.
[31] F. Ponzio, J. Barthès, J. Bour, M. Michel, P. Bertani, J. Hemmerlé, M. D'Ischia, V. Ball, *Chem. Mater.* **2016**, *28*, 4697.
[32] M. Salomäki, L. Marttila, H. Kivelä, T. Ouvinen, J. Lukkari, *J. Phys. Chem. B* **2018**, *122*, 6314.
[33] D. Kyoung Yeon, S. Ko, S. Jeong, S.-P. Hong, S. Min Kang, W. Kyung Cho, *Langmuir* **2019**, *35*, 1227.
[34] G. Brucheltc, V. A. Roginsky, P. Schuler, H. B. Stegmann, H. Köhle, *Z. Naturforsch. C* **2018**, *50*, 715.
[35] J. Liebscher, R. Mrówczyński, H. A. Scheidt, C. Filip, N. D. Haìdade, R. Turcu, A. Bende, S. Beck, *Langmuir* **2013**, *29*, 10539.
[36] E. Kaxiras, A. Tsolakidis, G. Zonios, S. Meng, *Phys. Rev. Lett.* **2006**, *97*, 218102.
[37] M. L. Tran, B. J. Powell, P. Meredith, *Biophys. J.* **2006**, *90*, 743.
[38] Y. Liu, K. Ai, J. Liu, M. Deng, Y. He, L. Lu, *Adv. Mater.* **2013**, *25*, 1353.
[39] E. Pastrana, *Nat. Methods* **2013**, *10*, 36.

[40] L. Zou, H. Wang, B. He, L. Zeng, T. Tan, H. Cao, X. He, Z. Zhang, S. Guo, Y. Li, *Theranostics* **2016**, *6*, 762.
[41] C. D. Spicer, C. Jumeaux, B. Gupta, M. M. Stevens, *Chem. Soc. Rev.* **2018**, *47*, 3574.
[42] A. Beck, L. Goetsch, C. Dumontet, N. Corvaïa, *Nat. Rev. Drug Discovery* **2017**, *16*, 315.
[43] C. L. Ventola, *Pharm. Ther.* **2017**, *42*, 742.
[44] J. Young Yhee, S. J. Lee, S. Lee, S. Song, H. S. Min, S.-W. Kang, S. Son, S. Y. Jeong, I. C. Kwon, S. H. Kim, K. Kim, S. Korea, *Bioconjugate Chem.* **2013**, *24*, 1850.
[45] D. Hauser, M. Estermann, A. Milosevic, L. Steinmetz, D. Vanhecke, D. Septiadi, B. Drasler, A. Petri-Fink, V. Ball, B. Rothen-Rutishauser, *Nanomaterials* **2018**, *8*, 1065.
[46] L. Zhu, J. Yu, Y. Xu, Z. Xi, B. Zhu, *Colloids Surf., B* **2009**, *69*, 152.
[47] D. Lapotko, *Nanomedicine* **2009**, *4*, 813.
[48] B. Vaz, V. Salgueiriño, M. Pérez-Lorenzo, M. A. Correa-Duarte, *Langmuir* **2015**, *31*, 8745.
[49] D. Maziukiewicz, B. Grześkowiak, E. Coy, S. Jurga, R. Mrówczyński, *Biomimetics* **2019**, *4*, 3.
[50] L.-C. Cheng, H. M. Chen, T.-C. Lai, Y.-C. Chan, R.-S. Liu, J. C. Sung, M. Hsiao, C.-H. Chen, L.-J. Her, D. P. Tsai, *Nanoscale* **2013**, *5*, 3931.
[51] T. K. Ryu, S. W. Baek, R. H. Kang, S. W. Choi, *Adv. Funct. Mater.* **2016**, *26*, 6428.
[52] T.-K. Ryu, S.-W. Baek, R.-H. Kang, K.-Y. Jeong, D.-R. Jun, S.-W. Choi, *J. Controlled Release* **2018**, *270*, 237.
[53] Y. Wu, A. Ermakova, W. Liu, G. Pramanik, T. M. Vu, A. Kurz, L. McGuinness, B. Naydenov, S. Hafner, R. Reuter, J. Wrachtrup, J. Isoya, C. Förtsch, H. Barth, T. Simmet, F. Jelezko, T. Weil, *Adv. Funct. Mater.* **2015**, *25*, 6576.
[54] L.-J. Su, M.-S. Wu, Y. Y. Hui, B.-M. Chang, L. Pan, P.-C. Hsu, Y.-T. Chen, H.-N. Ho, Y.-H. Huang, T.-Y. Ling, H.-H. Hsu, H.-C. Chang, *Sci. Rep.* **2017**, *7*, 45607.
[55] K. van der Laan, M. Hasani, T. Zheng, R. Schirhagl, *Small* **2018**, *14*, 1703838.